Synthetic gauge fields in synthetic dimensions: interactions and chiral edge modes

2016 New J. Phys. 18 035010

(http://iopscience.iop.org/1367-2630/18/3/035010)

New Journal of Physics
The open access journal at the forefront of physics

Deutsche Physikalische Gesellschaft DPG
IOP Institute of Physics

Published in partnership with: Deutsche Physikalische Gesellschaft and the Institute of Physics

OPEN ACCESS

RECEIVED
19 October 2015

REVISED
15 February 2016

ACCEPTED FOR PUBLICATION
19 February 2016

PUBLISHED
11 March 2016

PAPER

Synthetic gauge fields in synthetic dimensions: interactions and chiral edge modes

Simone Barbarino[1,6], **Luca Taddia**[2,3], **Davide Rossini**[1], **Leonardo Mazza**[4,1] and **Rosario Fazio**[5,1]

[1] NEST, Scuola Normale Superiore & Istituto Nanoscienze-CNR, I-56126 Pisa, Italy
[2] Scuola Normale Superiore, I-56126 Pisa, Italy
[3] CNR—Istituto Nazionale di Ottica, UOS di Firenze LENS, I-50019 Sesto Fiorentino, Italy
[4] Département de Physique, Ecole Normale Supérieure / PSL Research University, CNRS, 24 rue Lhomond, F-75005 Paris, France
[5] The Abdus Salam International Centre for Theoretical Physics (ICTP), I-34151 Trieste, Italy
[6] Author to whom any correspondence should be addressed.

E-mail: simone.barbarino@sns.it

Keywords: synthetic gauge fields, synthetic dimension, alkaline-earth(-like) atoms, interactions and nonlinear effects, density-matrix renormalization group and matrix-product states

Abstract

Synthetic ladders realized with one-dimensional alkaline-earth(-like) fermionic gases and subject to a gauge field represent a promising environment for the investigation of quantum Hall physics with ultracold atoms. Using density-matrix renormalization group calculations, we study how the quantum Hall-like chiral edge currents are affected by repulsive atom–atom interactions. We relate the properties of such currents to the asymmetry of the spin resolved momentum distribution function, a quantity which is easily addressable in state-of-art experiments. We show that repulsive interactions significantly enhance the chiral currents. Our numerical simulations are performed for atoms with two and three internal spin states.

1. Introduction

One of the most noticeable hallmarks of topological insulators is the presence of robust *gapless edge modes* [1]. Their first experimental observation goes back to the discovery of the quantum Hall effect [2], where the existence of chiral edge states is responsible for the striking transport properties of the Hall bars. The physics of edge states has recently peeked out also in the arena of ultracold gases [3–5], triggered by the new exciting developments in the implementation of topological models and synthetic gauge potentials for neutral cold atoms [6–10].

Synthetic gauge potentials in cold atomic systems have already led to the experimental study of Bose–Einstein condensates coupled to a magnetic field [11] or with an effective spin–orbit coupling [12], and more recently to lattice models with non-zero Chern numbers [13–16] and frustrated ladders [3]. In a cold-gas experiment, the transverse dimension of a two-dimensional setup does not need to be a *physical* dimension, i.e. a dimension in real space: an extra *synthetic* dimension on a given d-dimensional lattice can be engineered taking advantage of the internal atomic degrees of freedom (e.g. hyperfine or nuclear spin states) [17]. The crucial requirement is that each of them has to be coupled to two other states in a sequential way through, for example, proper Raman transitions induced by laser beams. In this situation, it is even possible to generate gauge fields in synthetic lattices [18].

In this work we focus on one-dimensional systems with a finite synthetic dimension coupled to a synthetic gauge field, i.e. *frustrated ladders*. The study of such ladders traces back to more than thirty years ago, when frustration and commensurate–incommensurate transitions have been addressed in Josephson networks [19, 20]. Thanks to the experimental advances with optical lattices, these systems are now reviving a boost of activity. Both bosonic (see, e.g., [21–26]) and fermionic (see, e.g., [27–36]) systems have been considered. The emerging phenomenology is very rich, ranging from new phases with chiral order [21] to vortex phases [24] or fractional Hall-like phases in fermionic systems [31, 33], just to give some examples.

Very recently, two experimental groups [4, 5] have observed persistent spin currents in one-dimensional gases of ^{173}Yb (fermions) and ^{87}Rb (bosons) induced by the presence of such gauge field. Within the framework of the synthetic dimension, spin currents appearing associated to the extremal spin states can be regarded as the *chiral* edge states of a two-dimensional system and are reminiscent of the edge modes of the Hall effect. Up to now, the study of spin-resolved currents in optical lattices has mainly focused on aspects related to the single-particle physics and a systematic investigation of the interaction effects is missing. Repulsive interactions considerably affect the properties of the edge modes of two-dimensional systems pierced by a magnetic flux: this is well known in condensed matter, where the fractional quantum Hall regime [37] can be reached for proper particle fillings and for sufficiently strong Coulomb interactions. In view of the new aforementioned experiments in bosonic [5] and fermionic [4] atomic gases, a deeper understanding of the role of repulsive interactions in these setups is of the uttermost importance.

Here we model the experiment on the frustrated n-leg ladder performed in [4] and analyze, by means of density-matrix renormalization group (DMRG) simulations, how atom–atom repulsive interactions modify the edge physics of the system (in this article we disregard the effects of an harmonic confinement and of the temperature). We concentrate on the helical part of the non-interacting spectrum of these systems and consider fermionic densities such that the chemical potential of the non-interacting model lies there. Here, low-energy excitations correspond to the extremal spin states which counter propagate and thus originate an helical liquid; in the synthetic-dimension framework such helical modes can be considered as chiral edge modes. This is the region of the spectrum where the analogy to a quantum Hall effect model is tighter (although the currents presented in this article do not have any topological origin).

The purpose of this article is twofold. First, we want to present numerical evidence that helical modes reminiscent of the chiral currents of the integer quantum Hall effect can be stabilized by repulsive interactions. Second, we want to discuss the influence of interactions on experimentally measurable quantities that witness the helicality of the modes. By slightly changing both the chemical potential and strength of the repulsive interaction, we highlight a number of noticeable consequences of interactions. To this aim, we focus on the momentum distribution function, which has already been used in the experiment reported in [4] to indirectly probe the existence of the spin-resolved currents. For ladders with two or three legs, probing the presence of spin-resolved currents is not sufficient to identify whether the system is in an helical phase. However we argue that this approach is sufficient in the case of ladders with a number of legs $n \gtrsim 4$, thus providing additional motivations for future experiments.

Before concluding the introduction, there is an important point to be stressed when dealing with synthetic ladders in the presence of interactions. The many-body physics of alkaline-earth(-like) atoms (like ytterbium) with nuclear spin I larger than $1/2$ is characterized by a SU$(2I+1)$ symmetry [38–40]. When they are viewed as $(2I+1)$-leg ladders, the interaction is strongly anisotropic, i.e. it is short-range in the physical dimension and long-range in the synthetic dimension. This situation is remarkably different from the typical condensed-matter systems and may lead to quantitative differences especially when considering narrow ladders, as in [4].

The paper is organized as follows. In the next section we introduce the model describing a one-dimensional gas of earth-alkaline(-like) atoms with nuclear spin $I \geqslant 1/2$. In order to make a clear connection with the experiment of [4], we briefly explain how this system can be viewed as a $(2I+1)$-leg ladder. Moreover, we present a discussion of the single-particle spectrum to understand the main properties of the edge currents in the non-interacting regime and to identify the regimes where the effects of repulsive interactions are most prominent. Then, in section 3 we introduce two quantities, evaluated by means of the DMRG algorithm, that characterize the edge currents: the (spin-resolved) momentum distribution function and the average current derived from it. In section 4 we present and comment our results; we conclude with a summary in section 5.

2. Synthetic gauge fields in synthetic dimensions

2.1. The model

We consider a one-dimensional gas of fermionic earth-alkaline-(like) neutral atoms characterized by a large and tunable nuclear spin I, see figure 1(a). Based on the predictions of [38], Pagano *et al* have experimentally shown that, by conveniently choosing the populations of the nuclear-spin states, the number of atomic species can be reduced at will to $2\mathcal{I}+1$, giving rise to an effective atomic spin $\mathcal{I} \leqslant I$ [41]. We stress that I has to be an half-integer to enforce the fermionic statistics, while $\mathcal{I}$ can also be an integer, see figure 1(b). Moreover, as extensively discussed in [17, 18], the system under consideration can be both viewed as a one-dimensional gas with $2\mathcal{I}+1$ spin states or as a $(2\mathcal{I}+1)$-leg ladder, see figure 1(c).

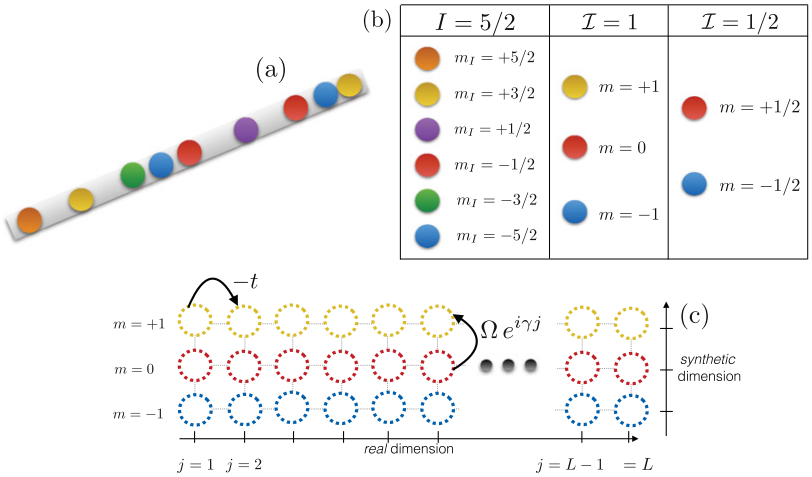

Figure 1. Implementation of $\hat{H} = \hat{H}_0 + \hat{H}_1$ in a cold-atom system. (a) Sketch of a one-dimensional atomic gas with nuclear spin $I = 5/2$, e.g. ^{173}Yb. (b) definition of the effective spins $\mathcal{I} = 1$ and $\mathcal{I} = 1/2$ as in the experimental implementation with ^{173}Yb of [4]. (c) Graphical representation of the non-interacting Hamiltonian in the synthetic-dimension picture, for the case $\mathcal{I} = 1$.

When atoms are loaded into an optical lattice, the Hamiltonian can be written as [38]:

$$\hat{H}_0 = -t\sum_{j}\sum_{m=-\mathcal{I}}^{\mathcal{I}}(\hat{c}^{\dagger}_{j,m}\hat{c}_{j+1,m} + \text{h.c.}) + U\sum_{j}\sum_{m<m'}\hat{n}_{j,m}\hat{n}_{j,m'}, \tag{1}$$

where $\hat{c}_{j,m}$ ($\hat{c}^{\dagger}_{j,m}$) annihilates (creates) a spin-m fermion ($m = -\mathcal{I},\ldots,\mathcal{I}$) at site $j = 1,\ldots,L$ and $\hat{n}_{j,m} = \hat{c}^{\dagger}_{j,m}\hat{c}_{j,m}$; t is the hopping amplitude, while U is the strength of the SU$(2\mathcal{I}+1)$-invariant interaction; the first sum in the hopping term runs over $j = 1,\ldots,L-1$ if open boundary conditions (OBC) in the real dimension are considered, or over $j = 1,\ldots,L$ if periodic boundaries (PBC) are assumed. Hereafter we set $\hbar = 1$. The Hamiltonian (1), also known as the SU$(2\mathcal{I}+1)$ Hubbard model, has attracted considerable attention in the last few decades, see e.g. [42–45].

The presence of two additional laser beams can induce a coupling between spin-states with $\Delta m = \pm 1$ of amplitude Ω_m endowed with a running complex phase factor $e^{i\gamma j}$ via adiabatic elimination of the excited state. The coupling Ω_m is related to the intensity of the laser beams and to the Clebsch–Gordan coefficients associated to the induced atomic transitions. Assuming that all the couplings are induced by the same pair of lasers, the dependence on m is only due to the mentioned Clebsch–Gordan coefficients, although nothing prevents the use of more sophisticated experimental schemes with several laser pairs, and thus the occurrence of more general situations. The phase γ depends on the laser-light wavelength and on the relative propagation angle of the two beams. Explicitly, the Hamiltonian gets a contribution of the form [18]

$$\hat{H}_1 = \sum_{j}\sum_{m=-\mathcal{I}}^{\mathcal{I}-1}\Omega_m(e^{-i\gamma j}\hat{c}^{\dagger}_{j,m}\hat{c}_{j,m+1} + \text{h.c.}). \tag{2}$$

As already mentioned, the system characterized by the Hamiltonian $\hat{H} \equiv \hat{H}_0 + \hat{H}_1$ is equivalent to a $(2\mathcal{I}+1)$-leg ladder where the coordinate in the transverse direction is given by the effective-spin index $m = -\mathcal{I},\ldots,\mathcal{I}$. For all purposes, such direction can be regarded as a synthetic dimension with sharp edges; in this framework, the Hamiltonian $\hat{H}_1$ describes the hopping in the synthetic dimension and introduces a constant magnetic field perpendicular to the ladder with dimensionless magnetic flux $+\gamma$ per plaquette. The peculiarity of our synthetic ladder resides in the interaction term, which is $SU(2\mathcal{I}+1)$ invariant: it therefore describes an on-site interaction in the real dimension and a long-range interaction in the synthetic one.

Since the Hamiltonian $\hat{H}$ is not translationally invariant, for later convenience, we perform the unitary transformation $\hat{d}_{j,m} = \hat{\mathcal{U}}\hat{c}_{j,m}\hat{\mathcal{U}}^{\dagger} = e^{-im\gamma j}\hat{c}_{j,m}$ such that $\hat{\mathcal{U}}(\hat{H}_0 + \hat{H}_1)\hat{\mathcal{U}}^{\dagger} = \hat{\mathcal{H}}_0 + \hat{\mathcal{H}}_1 = \hat{\mathcal{H}}$ reads

$$\hat{\mathcal{H}}_0 = -t\sum_{j}\sum_{m=-\mathcal{I}}^{\mathcal{I}}(e^{i\gamma m}\hat{d}^{\dagger}_{j,m}\hat{d}_{j+1,m} + \text{h.c.}) + U\sum_{j}\sum_{m<m'}\hat{\nu}_{j,m}\hat{\nu}_{j,m'}, \tag{3}$$

$$\hat{\mathcal{H}}_1 = \sum_{j}\sum_{m=-\mathcal{I}}^{\mathcal{I}-1}(\Omega_m\,\hat{d}^{\dagger}_{j,m}\hat{d}_{j,m+1} + \text{h.c.}), \tag{4}$$

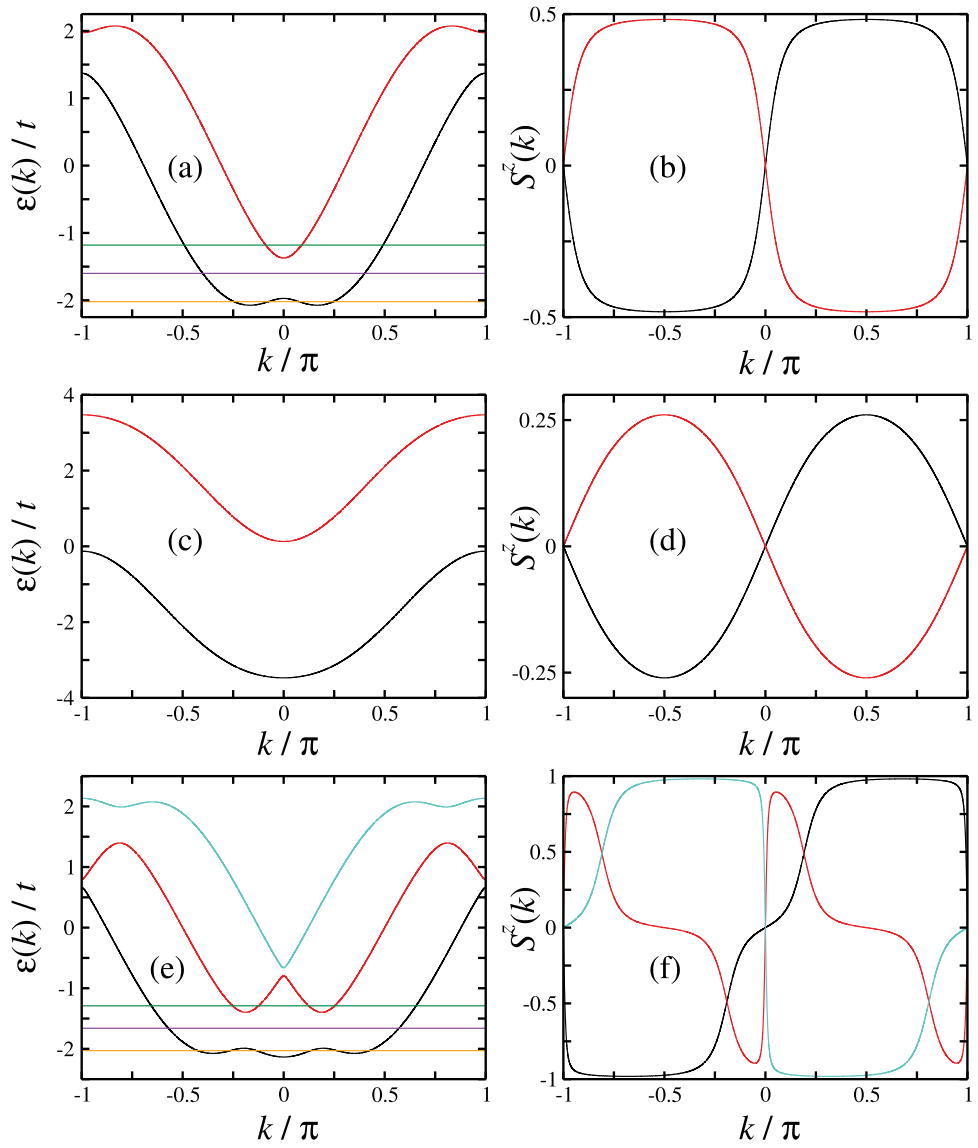

Figure 2. Spectral properties of $\hat{\mathcal{H}}$ in the non-interacting case. Left panels: energy spectra; right panels: spin polarization along the z-axis of the quasi-momentum single-particle eigenstates for several cases (lines with the same colors are in correspondence). Panels (a) and (b): $\mathcal{I} = 1/2$ and WRC regime ($\Omega/t = 0.3$). Panels (c) and (d): $\mathcal{I} = 1/2$ and SRC regime ($\Omega/t = 1.8$). Panels (e) and (f): $\mathcal{I} = 1$ and WRC regime ($\Omega/t = 0.1$). In all the situations, we assumed $\gamma = 0.37\pi$, PBC and $L \to \infty$. In panels (a) and (e), the orange, violet and green lines describe, respectively, the low-, intermediate- and high-filling situations considered in the text.

where $\hat{\nu}_{j,m} = \hat{d}^{\dagger}_{j,m}\hat{d}_{j,m}$. Assuming PBC in the real dimension, the quadratic part of $\hat{\mathcal{H}}$ can be diagonalized in Fourier space, in terms of the operators $\hat{d}_{p,m} = L^{-1/2}\sum_{j=1}^{L} e^{ik_p j}\hat{d}_{j,m}$, with $k_p = 2\pi p/L$ and $p \in \{-L/2, \ldots, L/2 - 1\}$.

2.2. Non-interacting helical liquid

In order to discuss the helical properties of this system, a good starting point is the analysis of the non-interacting physics for the $\mathcal{I} = 1/2$ case. The single-particle spectrum of the Hamiltonian $\hat{\mathcal{H}}$ has two branches with the following dispersion relations:

$$\epsilon_{\pm}(k_p) = -2t\cos\frac{\gamma}{2}\cos k_p \pm \sqrt{4t^2\sin^2\frac{\gamma}{2}\sin^2 k_p + \Omega^2}\,. \tag{5}$$

When the condition $\Omega < 2t\sin\frac{\gamma}{2}\tan\frac{\gamma}{2}$ is satisfied, the lower branch displays two minima at $k_p \approx \pm\gamma/2$ and a local maximum at $k_p = 0$, see figure 2(a): this case will be referred to as the weak-Raman-coupling (WRC) regime. In the opposite case, dubbed strong-Raman-coupling (SRC) regime, the lower branch has one single minimum at $k_p = 0$ without any special feature at $k_p \neq 0$, see figure 2(c).

The study of the spin polarization S^z (related to the operator $\sum_{j,m} m\,\hat{\nu}_{j,m}$) of each eigenmode highlights an important difference between the SRC and the WRC regimes (see figures 2(b) and (d)), although the polarization

of the single-particle modes depends continuously on Ω and no singularity appears when crossing from the WRC to the SRC regime. In the WRC case, for most of the values of k_p, the eigenstates are prevalently polarized along the z-direction, while in the SRC regime this is not true (the dominating polarization is along the x direction, not shown here). Figure 2(a) also shows that in the WRC regime depending on the filling, the low-energy excitation may have very different properties. For low (e.g. the orange line) or high (e.g. the green line) fillings, there are four low-energy excitations. However, when the chemical potential (here we consider zero temperature) lies between $-2t\cos(\gamma/2) - \Omega$ and $-2t\cos(\gamma/2) + \Omega$ (e.g. the violet line), there are two gapless excitations which have definite quasi-momentum and, in the limit $\Omega/t \to 0$, definite spin in the z direction. In the non-interacting case and for $\Omega/t \to 0$, this is an *helical liquid* which, once interpreted as a ladder, features two chiral edge modes.

Similar considerations about the single-particle spectrum hold for the $\mathcal{I} \geqslant 1$ cases, even though the analytic form of the eigenenergies is more involved. In figure 2(e) we show the single-particle energy spectrum of the eigenstates in the WRC regime for $\mathcal{I} = 1$ because of its experimental relevance [4]. Low, intermediate and high fillings can be identified also in this case, and are indicated by the three different horizontal lines. The intermediate filling (violet line) corresponds to the regime where the helical liquid appears; indeed the spin polarization S^z shown in figure 2(f) exhibits almost full polarization of the eigenstates close to the considered Fermi energy. For $\Omega/t \to 0$, in the synthetic-dimension representation, the three-leg ladder displays here chiral modes.

In the interacting case, the spectral properties of the Hamiltonian are not trivially computable. In the following section we define the physical quantities used to properly characterize the helical modes, which can be calculated by means of the DMRG algorithm. In the remainder of this paper we carefully analyze such quantities.

3. Observables

The study of the momentum distribution function, both spin-resolved and non-spin-resolved, can provide, as we shall see, information about the helical/chiral nature of the interacting liquid under consideration. The spin-resolved momentum distribution function is defined as

$$n_{p,m} = \langle \hat{c}^\dagger_{p,m}\hat{c}_{p,m}\rangle = \frac{1}{L}\sum_{j,l} \mathrm{e}^{-\mathrm{i}\frac{2\pi p}{L}(j-l)}\langle \hat{c}^\dagger_{j,m}\hat{c}_{l,m}\rangle, \tag{6}$$

where expectation values are taken over the ground state. Since p is not a good quantum number for $\hat{H}$, we will conveniently consider Hamiltonian $\hat{\mathcal{H}}$ and the momentum distribution function $\nu_{p,m} = \langle \hat{d}^\dagger_{p,m}\hat{d}_{p,m}\rangle$, for which it easy to verify that $\nu_{p,m} = n_{p-m\gamma,m}$. Accordingly, the total momentum distribution is given by $n_p = \sum_{m=-\mathcal{I}}^{\mathcal{I}} n_{p,m}$.

Based on these definitions, we introduce two observable quantities which identify the spin currents induced by the gauge field $\gamma \neq 0$, even in the presence of repulsive interactions. To this aim, we first solve the continuity equation for the Hamiltonian $\hat{H}$ and define the ground-state average chiral current

$$\mathcal{J}_{j,m} = -i\ t\ \langle \hat{c}^\dagger_{j,m}\hat{c}_{j+l,m}\rangle + \text{h.c.}. \tag{7}$$

Assuming PBC in the real dimension and using equation (6), its spatial average can be re-expressed as

$$Q_m = \frac{1}{L}\sum_j \mathcal{J}_{j,m} = -\frac{2t}{L}\sum_{p>0}\sin k_p\,(n_{p,m} - n_{-p,m}), \tag{8}$$

with $k_p = 2\pi p/L$. The latter relation allows to indirectly probe the existence of chiral currents using a quantity, namely $n_{p,m}$, which can be experimentally observed in state-of-art laboratories using a band-mapping technique [46] followed by a Stern–Gerlach–time-of-flight imaging [4, 5]. The quantity Q_m is the first observable to be employed in the following.

The second observable is the quantity

$$J_m = -\sum_{p>0}(n_{p,m} - n_{-p,m}), \tag{9}$$

defined in [4], which is more directly related to the asymmetry of the spin-resolved momentum distribution function.

When working in the gauge which has momentum as well-defined quantum number, see equations (3) and (4), it is convenient to express the two observables as follows:

$$Q_m = -\frac{2t}{L}\sum_{p>0}\sin k_p\,(\nu_{p+m\gamma,m} - \nu_{-p+m\gamma,m}), \tag{10}$$

$$J_m = -\sum_{p>0} (\nu_{p+m\gamma,m} - \nu_{-p+m\gamma,m}). \tag{11}$$

Both J_m and Q_m give information about the existence of circulating persistent currents in the system and, as we shall see below, display the same qualitative behavior (they only differ for a cut-off at low wavelength). However, it is important to stress that measuring non-zero values of Q_m and J_m is not sufficient to identify that the system is in an helical phase. To this aim, the comparison of the values of Q_m (or J_m) for several values of m is necessary. In particular, an helical phase should display a value of $|Q_m|$ (or $|J_m|$) which decreases while the absolute value of m is decreased and thus, within the synthetic-dimension framework, one moves away from the edges towards the bulk. Only provided this condition is fulfilled one can speak of an *helical* liquid (or correspondingly a *chiral* ladder). Unfortunately, for $\mathcal{I} = 1/2$ and $\mathcal{I} = 1$, the situations experimentally realized in [4], this comparison cannot be done because of the reduced size of the synthetic dimension. Here, the quantities in equations (8) and (9) can only be used to diagnose the spin currents of the system.

4. Results

Equipped with the definitions given in the previous sections, we now discuss how atom–atom repulsive interactions affect the momentum distribution functions n_p and $n_{p,m}$ and the observables Q_m and J_m for $\mathcal{I} = 1/2$ and $\mathcal{I} = 1$ [4]. The results for the non-interacting cases, here used as a reference, are computed by means of an exact diagonalization technique which exploits the advantages offered by free fermionic theories. For interacting problems, $U/t \neq 0$, we rely on the DMRG algorithm [47, 48]. We only address the ground-state properties, i.e. rigorously work at zero temperature. In the finite-size sweeping procedure, up to 250 eigenstates of the reduced density matrix are kept, in order to achieve a truncation error of the order of 10^{-6} (in the worst cases) and a precision, for the computed correlations, at the fourth digit. The resulting inaccuracy is negligible on the scale of all the figures shown hereafter.

For simplicity, in the present discussion, we have assumed that Ω_m does not depend on m and set $\Omega_m = \Omega$. This assumption, which is relevant only for $\mathcal{I} = 1$, is equivalent to neglecting small experimental details on the Raman coupling between different spins. We do not expect this choice to introduce qualitative changes to the physics of the model as we are speaking of small differences which do not affect the order-of-magnitude of the couplings, as highlighted in [4] in the non-interacting regime.

Unless differently specified, in the $\mathcal{I} = 1/2$ case we consider $L = 96$ and $\Omega/t = 0.3$, while in the $\mathcal{I} = 1$ case we set $L = 48$ and $\Omega/t = 0.1$ (the ratio Ω/t is chosen in order to be in the WRC regime). As shown in figures 2(a) and (e), in the non-interacting regime we can outline three inequivalent classes of fillings that we dub low, intermediate and high. As we are interested in the discussion of the features of the interactions on the gases at low, intermediate and high fillings (see figure 2), we choose one specific value of the flux, $\gamma = 0.37\pi$, which has been used in the experiment in [4]. Accordingly, we consider $N/L = 3/16, 3/8$ and $7/12$ for $\mathcal{I} = 1/2$, and $N/L = 1/4, 13/24$ and $5/6$ for $\mathcal{I} = 1$ corresponding to the low-, intermediate-, and high-filling cases respectively. OBC in the real dimension have been adopted.

4.1. Momentum distribution functions

Let us first focus on the $\mathcal{I} = 1/2$ case. In figures 3(a)–(c) we plot the momentum distribution function ν_p for the three fillings listed above. For $U/t = 0$, the behavior of ν_p can be easily predicted by looking at the single-particle spectrum and the calculation is performed with an exact diagonalization exploiting the properties of free fermions. In the low and high-filling cases, peaks arise in correspondence of the partially occupied energy wells, while in the intermediate-filling case a more homogeneous momentum distribution function emerges.

The presence of repulsive atom–atom interactions significantly modifies the momentum distribution functions in the low- and high-filling cases: when U/t is increased, they drive the distribution towards a more homogeneous shape with enhanced tails, a typical effect of interactions [49]. In particular, the results in figures 3(a) and (c) hint at the fact that, provided the interaction is sufficiently strong, even low- and high-filling setups can be driven into a liquid with only two gapless modes (rather than four). This can be deduced by the fact that the number of Fermi edges, naively identified with the sharp discontinuities in ν_p as a function of p, is reduced from four to two. On the contrary, in the intermediate-filling case the homogeneous behavior is unmodified, apart from the mentioned tails.

Such a phenomenology can be explained, in certain regimes, using bosonization and renormalization-group techniques, as discussed in [50], where the effective low-energy theory of the model is derived in the perturbative limit $\Omega/t \to 0$. Interactions are shown to lead to an effective enhancement of the energy of the two gapped modes, whose absence characterizes the helical liquid. Thus, the interacting system is predicted to behave effectively as a free system where Ω/t is renormalized and increased, thus enhancing the range of fillings for which an helical liquid can be expected. Within this framework, the low- and high-filling setups encounter a

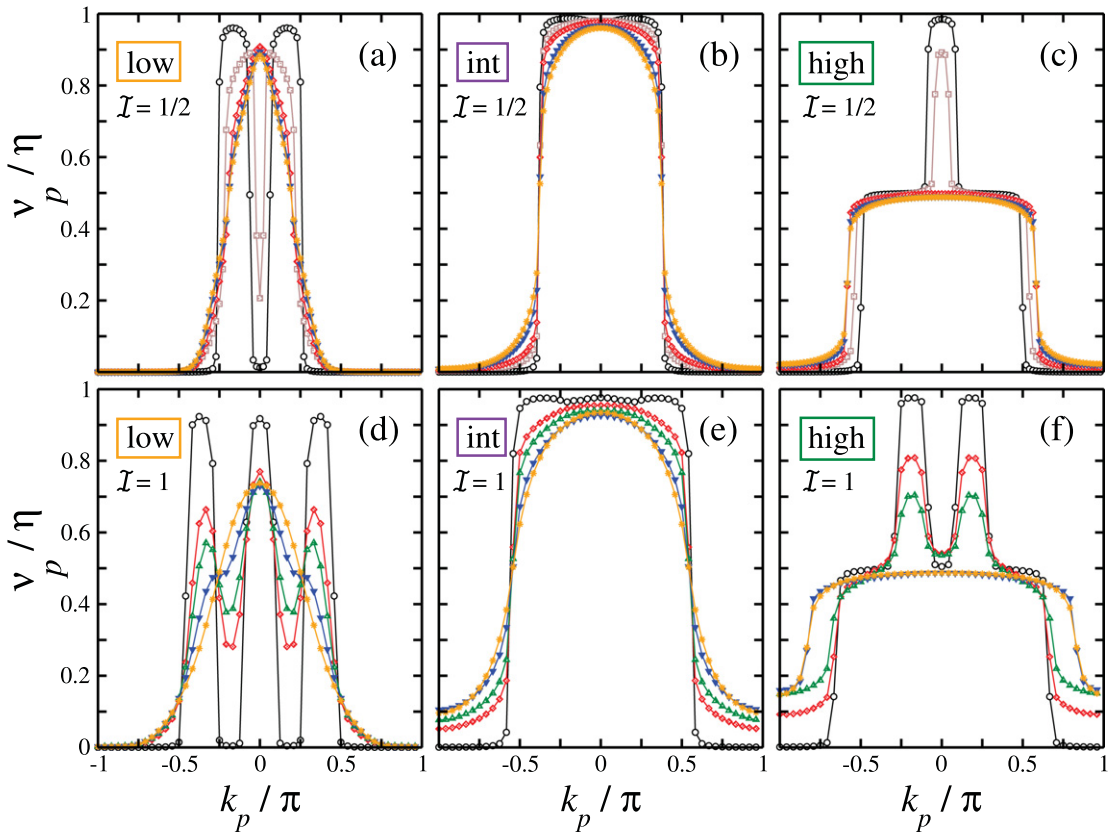

Figure 3. Momentum distribution functions ν_p for different values of the interaction coefficient. First row: $\mathcal{I} = 1/2$; second row: $\mathcal{I} = 1$. First column: low-filling case ($\eta = 1$); second column: intermediate-filling case ($\eta = 1$); last column: high-filling case ($\eta = 2$). The various colors denote different U/t values: 0 (black circles), 3 (brown squares), 5 (red diamonds), 8 (green triangles up), 20 (blue triangles down), $U/t \to \infty$ (orange stars).

phase transition as a function of U/t when switching from four to two low-lying modes. The detailed characterization of such phase transition is left for future work.

The results in figures 3(a) and (c) are consistent with this low-energy prediction, and in particular with the fact that repulsive interactions enhance the gap protecting the non-interacting helical liquid. However, it should be stressed that bosonization results are valid only for $\Omega/t \to 0$. As discussed at the end of section 3, the momentum distribution function is not sufficient to discuss whether increasing U/t the helical nature of the gapless modes at $U/t = 0$ is modified.

The momentum distribution functions for $\mathcal{I} = 1$ at the three mentioned fillings display the same qualitative behavior, see figures 3(d)–(f). Again, the underlying physics can be explained in terms of an effective enhancement of Ω/t, due to the presence of interactions.

It is important to note that in the SRC regime on-site interactions are not expected to significantly modify the momentum distribution function of the non-interacting system. This especially holds in the limit $\Omega/t \to \infty$. The occupied single-particle states belong only to the lowest band and are almost polarized in the same direction, x: the gas is thus quasi-spinless and an on-site interaction should only weakly alter the ground state because of Pauli exclusion principle.

Further information about the system can be revealed by the spin-resolved momentum distribution functions $\nu_{p,m}$. In figures 4(a)–(c) we plot such functions in the WRC regime for the spin species $m = 1/2$ and $\mathcal{I} = 1/2$. Such profiles are clearly asymmetric with respect to $k_p = 0$, indicating the helical nature of the ground state. Note that the asymmetry is enhanced by the interactions. A similar behavior is observed for $m = \pm 1$ and $\mathcal{I} = 1$, see figures 4(d)–(f). On the other hand, for symmetry reasons, the momentum distribution function $\nu_{p,m=0}$ is symmetric with respect to $k_p = 0$, although it is modified by the interactions, see figures 4(g)–(i).

4.2. Spin-resolved current

In this paragraph we discuss the properties of the quantities Q_m and J_m defined in section 3 for an interacting system. Even though a preliminary analysis of these quantities has been carried out in [31], a systematic study of the effects of repulsive atom–atom interactions in a relevant experimental setup [4] is still lacking.

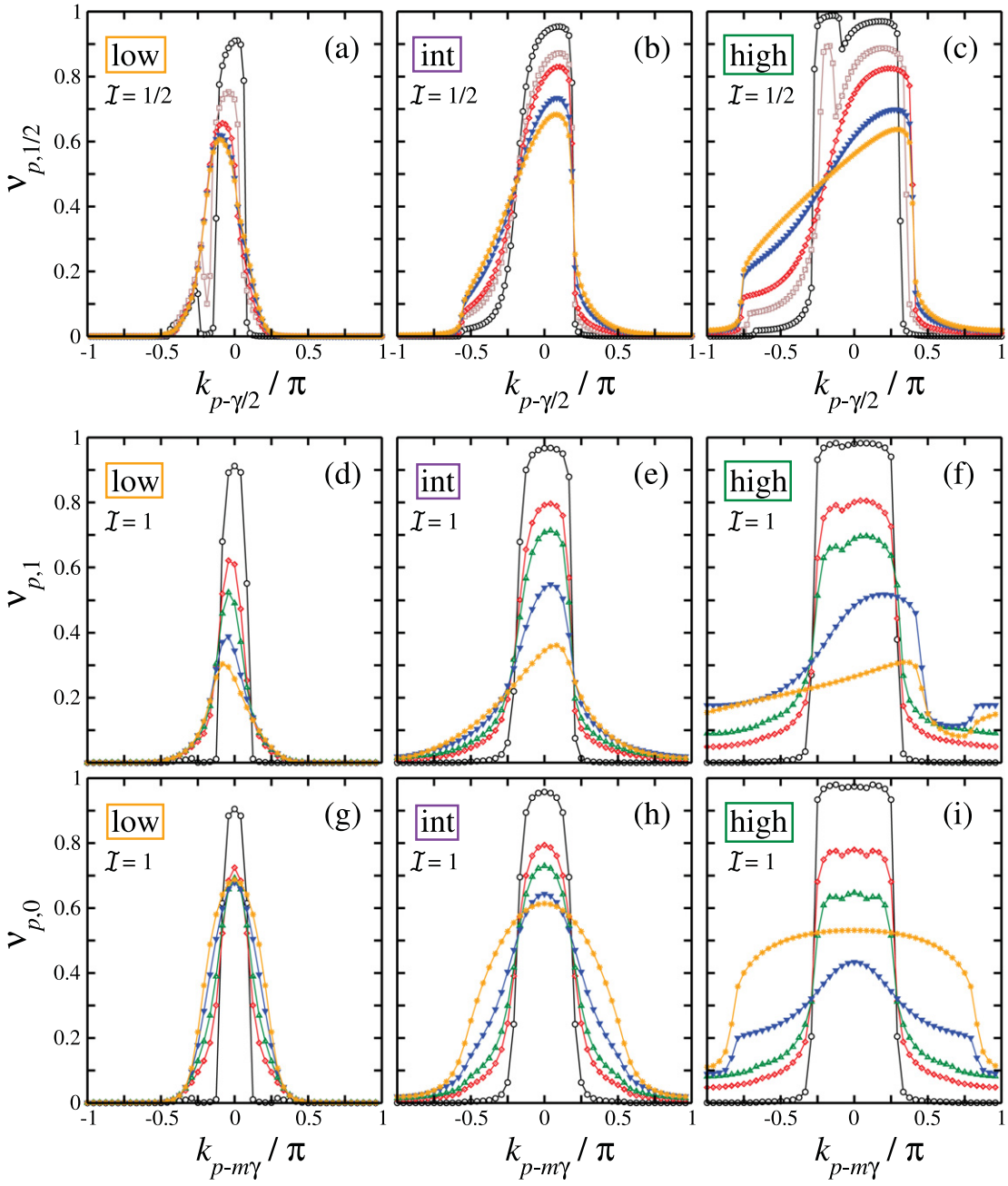

Figure 4. Spin-resolved momentum distribution functions $\nu_{p,m}$ for different values of U/t in the WRC regime. First row: $\mathcal{I} = 1/2$ (note that $\nu_{p,-1/2} = \nu_{-p,1/2}$); second and third row: $\mathcal{I} = 1$ (note that $\nu_{p,-1} = \nu_{-p,1}$). Panels (a), (d) and (g): low-filling case; panels (b), (e) and (h): intermediate-filling case; panels (c), (f) and (i): high-filling case. For the color code, see the caption of figure 3.

In figures 5(a) and (c) we display the behavior of $Q_{m=\mathcal{I}}$ as a function of U for the cases $\mathcal{I} = 1/2$ and $\mathcal{I} = 1$; we focus again on the three fillings outlined above. In appendix we show that, although the system has OBC and it is not homogeneous, averaging over many lattice sites yields a value related to the bulk current. A first striking observation is that one can observe different trends, also displaying non-monotonic features. The role of interactions in enhancing the persistent currents of the system here encounters a first naive confirmation: in all cases, the value of $|Q_m|$ in the $U/t \to \infty$ limit exceeds that of the non-interacting system.

In order to understand the dependence of Q_m on U/t, we employ an effective model. We have already noticed that the most prominent effect of the interactions on ν_p is that of letting the system behave as if it were non-interacting but with a renormalized value of Ω. Here we test this observation by studying the dependence of Q_m on Ω in the absence of interactions. Results displayed in figures 5(b) and (d) show that this simple model offers a good qualitative understanding of the interacting system. For example, in both the $\mathcal{I} = 1/2$ and $\mathcal{I} = 1$ cases, $Q_{m=\mathcal{I}}$ displays the same (quasi-)monotonic increasing behavior with U/t and with Ω/t, for the low and intermediate fillings. In the high-filling case, $Q_{m=\mathcal{I}}$ exhibits a strongly non-monotonic behavior as a function of

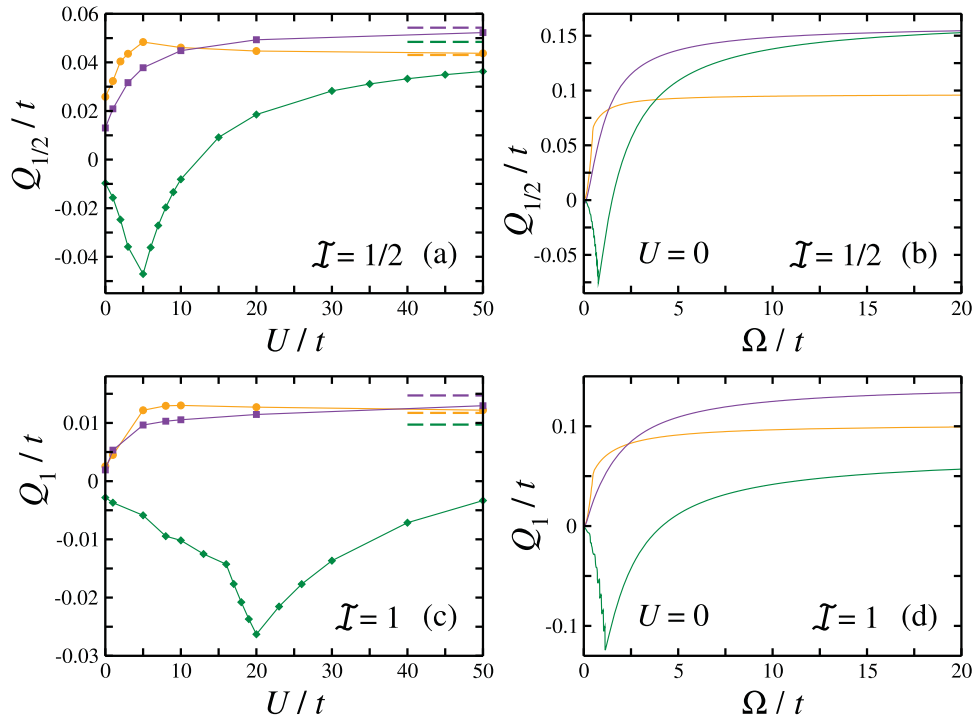

Figure 5. Dependence of $Q_{m=\mathcal{I}}$ on the interaction strength. Panel (a): $Q_{1/2}$ for $\mathcal{I}=1/2$ as a function of the interaction strength U/t; dashed lines are the values of $Q_{1/2}$ in the limit $U/t\to\infty$. Panel (b): $Q_{1/2}$ for $\mathcal{I}=1/2$ in the non-interacting case ($U/t=0$) for different values of Ω/t. Panels (c) and (d): same analysis for $\mathcal{I}=1$ and $m=1$. The various curves denote the different regimes of low (orange circles), intermediate (violet squares) and high (green diamonds) filling.

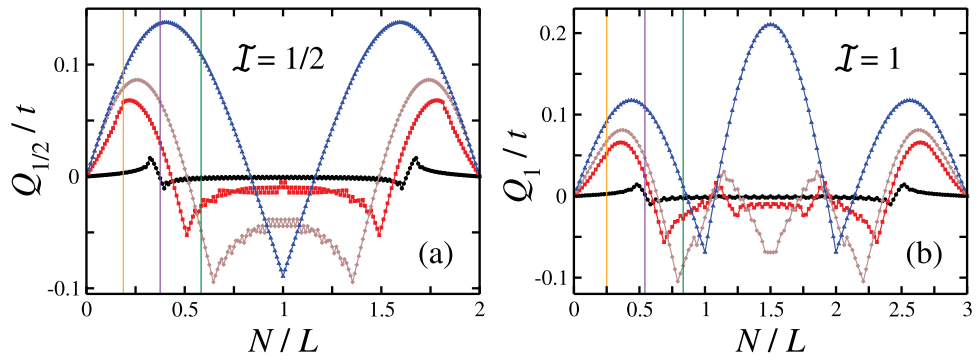

Figure 6. Spatially averaged currents as a function of the density of atoms. Panel (a): $Q_{1/2}$ for $\mathcal{I}=1/2$ in the non-interacting case and for different values of Ω (black: $\Omega=0.1$, red: $\Omega=0.5$, brown: $\Omega=1$, blue: $\Omega=5$); vertical lines mark low, intermediate and high fillings, with the same color code as in figure 2(a). Panel (b): same analysis for $\mathcal{I}=1$ and $m=1$.

U; in particular the plot points out a change in sign which is *a priori* unexpected because in the classical case the magnetic field determines unambiguously the direction of the circulating currents.

To further elucidate this problem, in figure 6 we plot the dependence of Q_m on the filling N/L for a fixed value of Ω/t and $U/t=0$ (see [33] for an analytic calculation for $\mathcal{I}=1/2$ with periodic boundary conditions). The plot shows that at low fillings the value of $Q_{m=\mathcal{I}}$ increases gently, but experiences an abrupt decrease once the helical region is entered, marked by the violet line (intermediate fillings). For higher fillings (even outside the helical region) and for small Ω, the value of $Q_{m=\mathcal{I}}$ is negative and thus the current changes sign; however, by increasing Ω, $Q_{m=\mathcal{I}}$ also increases, crossing 0 and becoming positive and finite. It thus follows that in this system there are single-particle states which are (i) antichiral (i.e. with opposite current flow) and (ii) which occur at accessible energies.

The quantity $J_{m=\mathcal{I}}$ shares many similarities with $Q_{m=\mathcal{I}}$. In figure 7 we plot $J_{m=\mathcal{I}}$ as a function of U, to be compared with figures 5(a) and (c) for $Q_{m=\mathcal{I}}$. Again, in the low- and intermediate-filling regimes $J_{m=\mathcal{I}}$ is almost

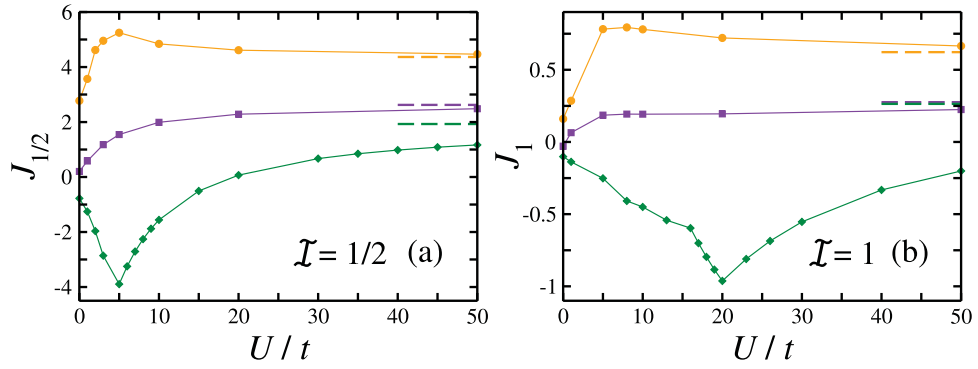

Figure 7. Dependence of $J_{m=\mathcal{I}}$ on the interaction strength. Panel (a): $Q_{1/2}$ for $\mathcal{I} = 1/2$ at low (orange circles), intermediate (violet squares) and high filling (green diamonds) as a function of the interaction strength U/t; dashed lines denote the values of $J_{1/2}$ in the limit $U/t \to \infty$. Panel (b): same analysis for $\mathcal{I} = 1$ and $m = 1$.

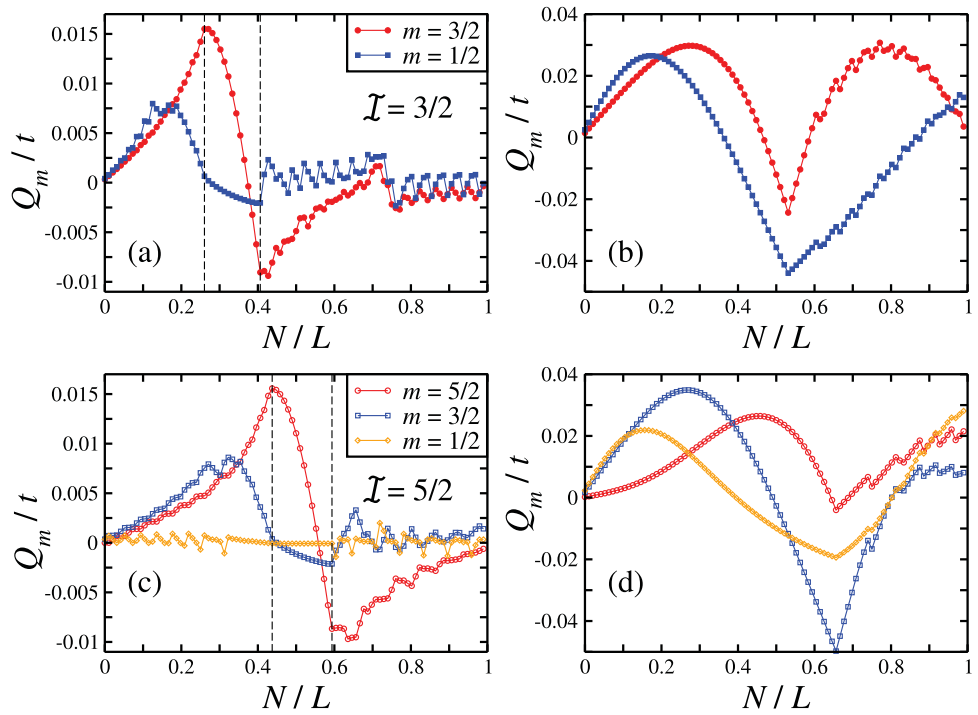

Figure 8. Evaluation of Q_m as a function of N/L for the non-interacting case $U/t = 0$, $\mathcal{I} = 3/2$ and $\mathcal{I} = 5/2$ in several parameter regimes. $L = 96$ and $\gamma = 0.19\pi$. Panel (a): $\mathcal{I} = 3/2$ and $\Omega/t = 0.1$ (WRC); panel (b) $\mathcal{I} = 3/2$ and $\Omega/t = 1$ (SRC); panel (c): $\mathcal{I} = 5/2$ and $\Omega/t = 0.1$ (WRC); panel (d) $\mathcal{I} = 5/2$ and $\Omega/t = 1$ (SRC).

monotonous, whereas monotonicity is significantly broken for high fillings. The explanation of this behavior can again be sought in the peculiar dependence of the current carried by the eigenmodes of the system.

4.3. Identifying the helical regime with spin-resolved currents

Before concluding, we briefly discuss the possibility of using the observables Q_m and J_m to detect a helical phase in a system with $\mathcal{I} > 1$. In figure 8 we consider the cases $\mathcal{I} = 3/2$ and $\mathcal{I} = 5/2$ and discuss, in the absence of interactions, the dependence on the filling of the quantities Q_m (similar results are expected for J_m). In panel (a) the system is tuned to the WRC regime, and the vertical lines highlight the helical region as computed from the single-particle eigenstates of the system. We observe that in this region the following properties are approximately true: $Q_{1/2} \sim 0$, and $Q_{3/2} \gtrsim Q_{1/2}$. This suggests that the measurement of spin-resolved currents can be useful to detect a region analogous to the chiral region of a quantum Hall effect. In panel (b) the system is tuned to the SRC regime and no helical phase is observed. Similar considerations hold when the number of legs is further increased, see panels (b) and (d) for $\mathcal{I} = 5/2$.

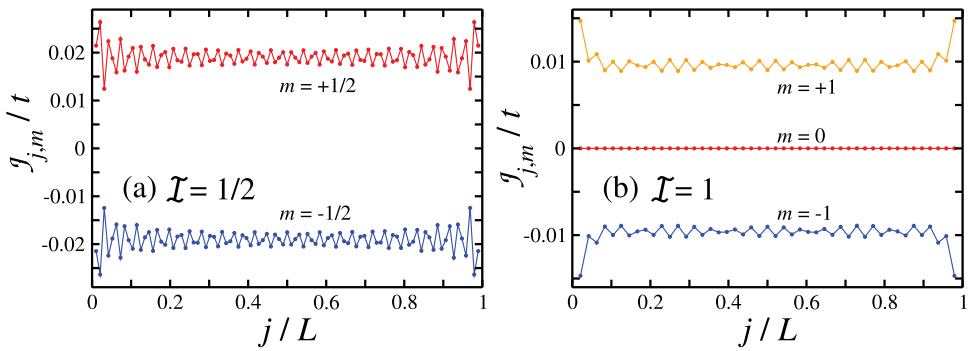

Figure A1. Spatial profile of the spin-resolved currents $\mathcal{J}_{j,m}$. Panel (a): $\mathcal{I} = 1/2$ (blue: $m = -1/2$; red: $m = 1/2$). Panel (b): $\mathcal{I} = 1$ (blue: $m = -1$; red: $m = 0$; orange: $m = 1$). In both cases, intermediate filling and $U/t = 5$ were chosen. The color code refers to figure 1. The other parameters of the simulations are set as in section 4.

5. Conclusions

By means of DMRG simulations, we have studied the impact of atom–atom repulsive interactions on the quantum Hall-like chiral currents recently detected in [4, 5]. We have modeled the experimental setup of [4] and characterized the behavior of the edge currents through the asymmetry of the momentum distribution function.

We have considered different particle fillings and we have shown that the spin-resolved currents are strongly enhanced by the presence of atom–atom repulsive interactions. To better assess this effect, we have introduced two observable quantities, which are displayed in figures 5 and 7, where the currents are studied as a function of the interaction strength U/t for different particle fillings. Moreover, we have shown that the presence of chiral currents is a clear hint of the quantum Hall-like behavior of synthetic ladders. However, for ladders with a little number of legs, probing the existence of spin-resolved currents is not sufficient to conclude that the system is in an helical phase. We have argued that this approach is sufficient in the case of ladders with a number of legs $2\mathcal{I} + 1 \gtrsim 4$, thus providing additional motivations for future experiments.

In the analysis presented here we have neglected the role of an harmonic trapping confinement as well as finite-temperature effects. Their interplay with interactions and the edge physics highlighted so far is left for a future work.

The edge currents studied here do not have a topological origin. However, these synthetic ladders may support fractional quantum Hall-like states [31, 33], and it would be very interesting to understand how to explore this regime by means of the quantities discussed in the present paper. In particular it would be important to develop a complete characterization of how fractional quantization may emerge in a cold atomic setup [51, 52].

Acknowledgments

We thank Leonardo Fallani and Guido Pagano for enlightening discussions, and Stefano Sinigardi and Daniele Cesini for technical support. We acknowledge INFN-CNAF for providing us computational resources and support, and D Cesini in particular. We acknowledge financial support from the EU integrated projects SIQS and QUIC, from Italian MIUR via PRIN Project 2010LLKJBX and FIRB project RBFR12NLNA. LM was supported by LabEX ENS-ICFP: ANR-10-LABX-0010/ANR-10-IDEX-0001-02 PSL*. RF acknowledges the Oxford Martin School for support and the Clarendon Laboratory for hospitality during the completion of the work.

Appendix. Currents

The quantity Q_m is the space-average value of the expectation value of the current operator over the ground state of the system, $\mathcal{J}_{j,m}$. Whereas in a homogeneous system with PBC this value coincides with the expectation value of the current on every site, the effects of the boundaries in a system with OBC might play an important role.

In figure A1 we plot $\mathcal{J}_{j,m}$ both for a system with $\mathcal{I} = 1/2$ (panel (a)) and with $\mathcal{I} = 1$ (panel (b)). The important information contained in the figure is that even if the system is clearly inhomogeneous, the space pattern of $\mathcal{J}_{j,m}$ is that of a small and fast oscillation over a constant value, so that the space average is an

indicative quantity of the underlying physics. For both $\mathcal{I} = 1/2$ and $\mathcal{I} = 1$ the oscillations vanish in the limit $L \to +\infty$, see [31].

References

[1] Hasan M Z and Kane C L 2010 *Rev. Mod. Phys.* **82** 3045
Qi X-L and Zhang S-C 2011 *Rev. Mod. Phys* **83** 1057
[2] Prange R and Girvin S 1990 *The Quantum Hall Effect* (New York: Springer)
[3] Atala M, Aidelsburger M, Lohse M, Barreiro J T, Paredes B and Bloch I 2014 *Nat. Phys.* **10** 588
[4] Mancini M *et al* 2015 *Science* **349** 1510
[5] Stuhl B K, Lu H-I, Aycock L M, Genkina D and Spielman I B 2015 *Science* **349** 1514
[6] Dalibard J, Gerbier F, Juzeliūnas G and Öhberg P 2011 *Rev. Mod. Phys.* **83** 1523
[7] Struck J, Ölschläger C, Weinberg M, Hauke P, Simonet J, Eckardt A, Lewenstein M, Sengstock K and Windpassinger P 2012 *Phys. Rev. Lett.* **108** 225304
[8] Hauke P *et al* 2012 *Phys. Rev. Lett.* **109** 145301
[9] Goldman N, Juzeliunas G, Ohberg P and Spielman I B 2014 *Rep. Prog. Phys.* **77** 126401
[10] Goldman N and Dalibard J 2014 *Phys. Rev.* X **4** 031027
[11] Lin Y-J, Compton R L, Jiménez-García K, Porto J V and Spielman I B 2009 *Nature* **462** 628
[12] Lin Y-J, Jiménez-García K and Spielman I B 2011 *Nature* **471** 83
[13] Aidelsburger M, Atala M, Lohse M, Barreiro J T, Paredes B and Bloch I 2013 *Phys. Rev. Lett.* **111** 185301
[14] Miyake H, Siviloglou G A, Kennedy C J, Burton W C and Ketterle W 2013 *Phys. Rev. Lett.* **111** 185302
[15] Jotzu G, Messer M, Desbuquois R, Lebrat M, Uehlinger T, Greif D and Esslinger T 2014 *Nature* **515** 237
[16] Aidelsburger M, Lohse M, Schweizer C, Atala M, Barreiro J T, Nascimbene S, Cooper N R, Bloch I and Goldman N 2015 *Nat. Phys.* **11** 162
[17] Boada A, Celi A, Latorre J I and Lewenstein M 2012 *Phys. Rev. Lett.* **108** 133001
[18] Celi A, Massignan P, Ruseckas J, Goldman N, Spielman I B, Juzeliunas G and Lewenstein M 2014 *Phys. Rev. Lett.* **112** 043001
[19] Kardar M 1984 *Phys. Rev.* B **30** 6368
[20] Kardar M 1986 *Phys. Rev.* B **33** 3125
[21] Dhar A, Maji M, Mishra T, Pai R V, Mukerjee S and Paramekanti A 2012 *Phys. Rev.* A **85** 041602
Dhar A, Maji M, Mishra T, Pai R V, Mukerjee S and Paramekanti A 2013 *Phys. Rev.* B **87** 174501
[22] Petrescu A and Le Hur K 2013 *Phys. Rev. Lett.* **111** 150601
[23] Grusdt F and Höning M 2014 *Phys. Rev.* A **90** 053623
[24] Piraud M, Heidrich-Meisner F, McCulloch I P, Greschner S, Vekua T and Schollwöck U 2015 *Phys. Rev.* B **91** 140406(R)
[25] Tokuno A and Georges A 2014 *New J. Phys.* **16** 073005
[26] Greschner S, Piraud M, Heidrich-Meisner F, McCulloch I P, Schollwck U and Vekua T 2015 *Phys. Rev. Lett.* **115** 190402
[27] Narozhny B N, Carr S T and Nersesyan A A 2005 *Phys. Rev.* B **71** 161101(R)
[28] Carr S T, Narozhny B N and Nersesyan A A 2006 *Phys. Rev.* B **73** 195114
[29] Roux G, Orignac E, White S R and Poilblanc D 2007 *Phys. Rev.* B **76** 195105
[30] Sun G, Jaramillo J, Santos L and Vekua T 2013 *Phys. Rev.* B **88** 165101
[31] Barbarino S, Taddia L, Rossini D, Mazza L and Fazio R 2015 *Nat. Commun.* **6** 8134
[32] Zeng T-S, Wang C and Zhai H 2015 *Phys. Rev. Lett.* **115** 095302
[33] Cornfeld E and Sela E 2015 *Phys. Rev.* B **92** 115446
[34] Mazza L, Aidelsburger M, Tu H-H, Goldman N and Burrello M 2015 *New J. Phys.* **17** 105001
[35] Budich J C, Laflamme C, Tschirsich F, Montangero M and Zoller P 2015 *Phys. Rev.* B **92** 245121
[36] Łacki M, Pichler H, Sterdyniak A, Lyras A, Lembessis V E, Al-Dossary O, Budich J C and Zoller P 2016 *Phys. Rev.* A **93** 013604
[37] Tsui D C, Stormer H L and Gossard A C 1982 *Phys. Rev. Lett.* **48** 1559
[38] Gorshkov A V, Hermele M, Gurarie V, Xu C, Julienne P S, Ye J, Zoller P, Demler E, Lukin M D and Rey A M 2010 *Nat. Phys.* **6** 289
[39] Cazalilla M A and Rey A M 2014 *Rep. Prog. Phys.* **77** 124401
[40] Capponi S, Lecheminant P and Totsuka K 2016 *Ann. Phys.* **367** 50
[41] Pagano G *et al* 2014 *Nat. Phys.* **10** 198
[42] Assaraf R, Azaria P, Caffarel M and Lecheminant P 1999 *Phys. Rev.* B **60** 2299
[43] Szirmai E and Sólyom J 2005 *Phys. Rev.* B **71** 205108
[44] Buchta K, Legeza Ö, Szirmai E and Sólyom J 2005 *Phys. Rev.* B **75** 155108
[45] Manmana S R, Hazzard K R A, Chen G, Feiguin A E and Rey A M 2011 *Phys. Rev.* A **84** 043601
[46] Köhl M, Moritz H, Stöferle T, Günter K and Esslinger T 2005 *Phys. Rev. Lett.* **94** 080403
[47] White S R 1992 *Phys. Rev. Lett.* **69** 2863
[48] Schollwöck U 2011 *Ann. Phys.* **326** 96
[49] Giamarchi T 2003 *Quantum Physics in One-Dimension* (Oxford: Oxford University Press)
[50] Braunecker B, Japaridze G I, Klinovaja J and Loss D 2010 *Phys. Rev.* B **82** 045127
[51] Calvanese Strinati M *et al* in preparation
[52] Taddia L *et al* in preparation